


DEVELOPMENT OF RAIN AND SCINTILLATION MODELS  
AT KU-BAND IN SOUTHEAST ASIA TROPICAL COUNTRIES

by

MANDEEP SINGH A/L JIT SINGH

Thesis submitted in fulfillment of the requirements  
for degree of Doctor of Philosophy

May 2006



## ACKNOWLEDGEMENTS

Firstly, I would like to express my deepest thanks and gratitude to GOD for giving me the strength and persistence to complete my research work. It is all his blessing that the present thesis has been materialized. I also state my out most appreciation and gratitude to my supervisor, *Professor Dr. Syed Idris Syed Hassan* of the School of Electrical and Electronics Engineering, Universiti Sains Malaysia who has guided me through out my research. I would also like to extend my gratitude to *Mr. Abdul Latip* from the Microwave and RF Laboratory for his assistance in the data collection and technical support. My appreciation is also extended to *Mr. Thikumporn Boonchuck* from King Mongkut's Institute of Technology Ladkrabang (KMITL) Thailand, *Ir. Joko Suryana* from Insitute Technologi Bandung (ITB) Indonesia, *Mr. Jose Claro Monje* from Ateneo de Manila University (ADMU) Philippines and *Dr. Ramachandran* from University of South Pacific (USP) Fiji for the assistance in data collection. Finally an acknowledgement to Universiti Sains Malaysia and the Ministry of Public Management, Home Affairs, Posts and Telecommunication Japan (POST-Partners)

## TABLE OF CONTENTS

	Page
TITLE PAGE	i
ACKNOWLEDGEMENTS	ii
TABLE OF CONTENTS	iii
LIST OF TABLES	vii
LIST OF FIGURES	x
LIST OF SYMBOLS	xiv
ABSTRAK	xvi
ABSTRACT	xvii
<b>CHAPTER 1 INTRODUCTION</b>	
1.1 Background	1
1.2 Objectives of Research	6
1.3 Organization of the Thesis	6
<b>CHAPTER 2 RAINFALL RATE MODELS</b>	
2.1 Introduction	8
2.2 The Importance of Rainfall Rate	9
2.3 Rainfall in Tropical and Equatorial Regions	10
2.4 Prediction of Rainfall Attenuation	12
2.4.1 Prediction of Rainfall Attenuation using Equiprobability Method	14
2.5 Prediction of Tropospheric Scintillation	16
2.5.1 Theory of Tropospheric Scintillation	16
2.5.2 Theory of Turbulence-Induced Scintillation	17
2.5.3 Description of Scintillation Effects	19
2.6 Conversion of Rainfall Rate from Sixty-minutes to One-minute	21
2.6.1 Segal's Method	21
2.6.2 Burgueno's Method	22

2.6.3	Chebil and Rahman's Method	23
2.6.4	Joo's Method	24
2.6.5	Moupfouma's Method	25
2.7	One-minute Rainfall Rates Models	25
2.7.1	Dutton and Dougherty Rainfall Rate Model	25
2.7.2	KIT (Kitami Institute of Technology)Simplified Rainfall Rate Model	27
2.7.3	Morita Rainfall Rate Model	28
2.7.4	Moupfouma (refined) Rainfall Rate Model	28
2.7.5	Rice and Holmberg Rainfall Rate Model	29
2.7.6	Douglas and Sims Rainfall Rate Distribution	31
2.7.7	Crane Rainfall Rate Distribution	32
2.7.8	ITU Rainfall Rate Model	33
2.8	One-minute Rainfall Attenuation Models	34
2.8.1	CETUC Rainfall Attenuation Model	35
2.8.2	Crane Global Rainfall Attenuation Model	35
2.8.3	DAH and ITU Rainfall Attenuation Model	37
2.8.4	Flavin Rainfall Attenuation Model	38
2.8.5	Gracia Lopez Rainfall Attenuation Model	39
2.8.6	Lin Rainfall Attenuation Model	40
2.8.7	Moupfouma Rainfall Attenuation Model	40
2.8.8	Yamada Rainfall Attenuation Model	41
2.8.9	Ong and Choo Rainfall Attenuation Model	42
2.8.10	Assis (refined) Rainfall Attenuation Model	43
2.8.11	Simple Attenuation Model (SAM Model)	43
2.9	Tropospheric Scintillation Models	44
2.9.1	ITU Tropospheric Scintillation Model	45
2.9.2	DPSP and MPSP Tropospheric Scintillation Model	45
2.9.3	Otung Tropospheric Scintillation Model	46

2.9.4	Kamp Tropospheric Scintillation Model	47
2.9.5	Karasawa Tropospheric Scintillation Model	48
2.9.6	Kamp-Tervonen-Salonen (KVS) Tropospheric Scintillation Model	49
2.9.7	Ortgies $N_{wet}$ and T Tropospheric Scintillation Model	50
2.10	Other Propagation Impairments	51
2.10.1	Atmospheric Attenuation	51
2.10.2	Cloud Attenuation	51
<b>CHAPTER 3 METHODOLOGY</b>		
3.1	Introduction	53
3.2	Rainfall Measurement System	54
3.2.1	The RS-102 Tipping Bucket Rain Gauge	55
3.2.2	The Casella Tipping Bucket Rain Gauge	56
3.3	Satellite Beacon Signal Measurement System	57
3.4	Calibration of the Instruments used for Measurement	60
3.4.1	Conversion of Rainfall Data to Rainfall Rate	62
3.4.2	Tipping Bucket Rain Gauge Calibration	63
3.4.3	Calibration of Beacon Monitor	65
3.5	Other Instruments Used	68
3.5.1	Humidity and Temperature Transmitter	68
3.5.2	Barometer Pressure Gauge	69
3.5.3	Wind Direction and Speed Transmitter	70
<b>CHAPTER 4 STASTICAL ANALYSIS RAINFALL AND SCINTILLATION PREDICTION MODELS</b>		
4.1	The Variation of Rainfall Amount	71
4.2	Rainfall Analysis	73
4.2.1	Percentage of Time Calculation	73
4.3	Error Analysis	74
4.3.1	The Uncertainty of Measurements	74

4.3.2	Regression Residual	75
4.4	Statistical Confidence Level	76
4.5	Test of The Prediction Models	78
4.5.1	RMS Percentage Error	78
4.6	Calculation of the Confidence Level and Interval of the Measured Data	79
4.7	Analysis of 60-Minutes Rainfall Rate Conversion Results	83
4.8	Analysis of 1-Minutes Rainfall Rate Measured Data with Existing Models	88
4.9	Analysis of 1-Minutes Rainfall Attenuation Measured Data with Existing Models	95
4.10	Analysis of Tropospheric Scintillation Measured Data with Existing Models	104
4.11	The Effect of Wind on Rain	108
4.12	Propagation Impairment caused by Atmospheric and Cloud Attenuation	114
<b>CHAPTER 5 DEVELOPMENT OF RAINFALL RATE, RAINFALL ATTENUATION AND SCINTILLATION MODELS</b>		
5.1	1-Minute Two-Part Rainfall Rate Model	116
5.2	Applying the Two-Part Model for Different Measurement Site	124
5.3	Rainfall Attenuation Model	128
5.4	Applying the Proposed Rainfall Attenuation Model at Different Locations	139
5.5	Tropospheric Scintillation Model	142
<b>CHAPTER 6 CONCLUSIONS</b>		
6.1	Conclusions	151
6.2	Recommendation for Future Study	152
<b>REFERENCES</b>		155
<b>APPENDIX A RAINFALL RATE CLIMATIC REGIONS</b>		169
<b>APPENDIX B MEASUREMENT INSTRUMENTS</b>		172
<b>APPENDIX C RESULTS IN TERMS OF TABLE AND FIGURE</b>		174
<b>APPENDIX D MATLAB CODING</b>		214

## LIST OF TABLES

	PAGE	
Table 2.1	Regression coefficients for estimating specific attenuation in equation (3.2). (Recommendation ITU-R P.838-1, 2001).	14
Table 2.2	ITU annual cumulative rainfall rate distribution for zones P and N (ITU-R P.837-3, 2001)	34
Table 3.1	Satellite specifications	59
Table 3.2	Antenna and site specifications	60
Table 3.3	Calibration of tipping bucket rain gauge	65
Table 3.4	The conversion coefficients (a, b) of voltage (V) into power (dBm)	66
Table 3.5	Calibration of beacon monitor	67
Table 3.6	Comparison of the measured temperature and humidity using digital meter and Humicap and Pt100 $\Omega$ resistance thermometer	69
Table 4.1	Wind effect on rainfall rate at different levels	112
Table 5.1	Comparison of long-term and short-term data	116
Table 5.2	Rainfall rate at different percentage of time divided by rainfall rate at 0.01% percentage of time for 10 stations year data.	117
Table 5.3	The Regression Coefficient for Power law and Log-normal equations	120
Table 5.4	The RMS error and residual of the Two-part model	121
Table 5.5	Percentage error and RMS error between the measured data and the model	125
Table 5.6	Rainfall rate and attenuation at 0.01% percentage of time averaged for both the years at USM, KMITL, ITB, USP and AdMU.	131
Table 5.7	The calculate values for slant path length and specific attenuation	132
Table 5.8	Comparison of the calculated and measured rainfall attenuation at 0.01% of time.	134
Table 5.9	The values for a,b and residual	135
Table 5.10	Comparison of the 2 years rainfall attenuation measured values with the proposed model values for USM, KMITL and ITB.	136
Table 5.11	Comparison of the 2 years rainfall attenuation measured values with the proposed model values for AdMU and USP	136
Table 5.12	Comparison between the proposed rainfall attenuation model with the data obtain from Lae, Rio de Janerio and Curitiba.	141

Table 5.13	Temperature and Humidity for 2 years	143
Table 5.14	The calculated values for $N_{wet}$ and $\sigma_{ref}$ for 2 years data	144
Table 5.15	The measured standard deviation for 2 years	145
Table 5.16	The calculated value for elevation angle scaling factor, $a$	146
Table 5.17	Measured scintillation amplitude values for different percentage of time	147
Table 5.18	Comparison between the measured standard deviation and proposed standard deviation using equation (5.11)	149
Table 5.19	Comparison of annual scintillation depth of calculated and measured data for 2 years.	149
Table A1	Point rainfall rate (mm/h) versus percent of year rainfall rate is exceeded for regions (Crane, 1980)	169
Table C1	Z score Statistical Table	179
Table C2	Evaluation results of sixty minutes rainfall rate models at USM for 2 years	180
Table C3	Evaluation results of sixty minutes rainfall rate models at KMITL for 2 years	180
Table C4	Evaluation results of sixty minutes rainfall rate models at USP for 2 years	181
Table C5	Evaluation results of sixty minutes rainfall rate models at ITB for 2 years	181
Table C6	Evaluation results of sixty minutes rainfall rate models at AdMU for 2 years	182
Table C7	Evaluation result of 1-minute rainfall rate models at USM for 2 years	190
Table C8	Evaluation result of 1-minute rainfall rate models at KMITL for 2 years	190
Table C9	Evaluation result of 1-minute rainfall rate models at USP for 2 years	191
Table C10	Evaluation result of 1-minute rainfall rate models at ITB for 2 years	191
Table C11	Evaluation result of 1-minute rainfall rate models at AdMU for 2 years	192
Table C12	Evaluation result of rainfall attenuation models at USM for 2 years	198
Table C13	Evaluation result of rainfall attenuation models at KMITL for 2 years	199
Table C14	Evaluation result of rainfall attenuation models at USP for 2 years	200

Table C15	Evaluation result of rainfall attenuation models at ITB for 2 years	201
Table C16	Evaluation result of rainfall attenuation models at AdMU for 2 years	202
Table C17	Evaluation results for enhancement signal at USM for 2 years	204
Table C18	Evaluation results for fade signal at USM for 2 years	204

## LIST OF FIGURES

		PAGE
Figure 2.1	Stratiform rainfall situations	11
Figure 2.2	Convective rainfall situations	11
Figure 2.3	Procedure for finding equal-probability value of attenuation, A and rainfall rate, R	15
Figure 2.4	Schematic of stratified and turbulent conditions in boundary layer of the atmosphere.	17
Figure 2.5	Contours of the coefficient $\beta$ for use in Rice-Holmberg model	30
Figure 2.6	Average rainfall rate-frequency relationships for four rain climates (Tattelman and Grantham, 1985)	32
Figure 3.1	Data collection set up in USM, USP, AdMU, ITB and KMITL	54
Figure 3.2	Beacon signal measurement setup for USM, AdMU, KMITL, USP and ITB	58
Figure 3.3	Calibration of the tipping bucket rain gauge	64
Figure 3.4	Beacon monitor calibration setup	65
Figure 3.5	Scatter plot for beacon monitor calibration	66
Figure 4.1	Measurement error range for the measured 2 years rainfall rate data	79
Figure 4.2	The confidence limits for the 2 years rainfall rate data	80
Figure 4.3	Measurement error range for the measured 2 years rainfall attenuation data	80
Figure 4.4	The confidence limits for the 2 years rainfall attenuation data	80
Figure 4.5	Measurement error range for the measured 2 years scintillation data	81
Figure 4.6	The confidence limits for the 2 years scintillation data	81
Figure 4.7	The MMS data in between 95% confidence limits of the measured data	83
Figure 4.8	The KMITL long-term data and 95% confidence limits of KMITL 2 years data	83
Figure 5.1	Rainfall Rate follows a power law distribution	117
Figure 5.2	Rainfall Rate follows a log-normal distribution	118
Figure 5.3	Percentage error of the two-part rainfall rate model for two years	120
Figure 5.4	Comparison of the two-part model with the measured data at USM	122

Figure 5.5	Comparison of the two-part model with the measured data at KMITL	122
Figure 5.6	Comparison of the two-part model with the measured data at ITB	123
Figure 5.7	Comparison of the two-part model with the measured data at USP	123
Figure 5.8	Comparison of the two-part model with the measured data at AdMU	123
Figure 5.9	Comparison of the two-part model with the rainfall rate data at Paya Lebar	126
Figure 5.10	Comparison of the two-part model with the rainfall rate data at de Janerio	127
Figure 5.11	Comparison of the two-part model with the rainfall rate data at S Paulo	127
Figure 5.12	Schematic diagram used to calculate the horizontal projection $L_g$ of the slant-path length (ITU-R PN.618-3, 1994).	129
Figure 5.13	Measured $L_G$ values plotted against calculated, $L_G$ values using equation (5.6).	133
Figure 5.14	Comparison of the proposed model with the measured data at USM	137
Figure 5.15	Comparison of the proposed model with the measured data at KMIT	137
Figure 5.16	Comparison of the proposed model with the measured data at ITB	137
Figure 5.17	Comparison of the proposed model with the measured data at AdMU	138
Figure 5.18	Comparison of the proposed model with the measured data at USP	138
Figure 5.19	Comparison between the proposed model with the data from Lae	140
Figure 5.20	Comparison between the proposed model with the data from Rio Janerio	140
Figure 5.21	Comparison between the proposed model with the data Curitiba	140
Figure 5.22	The coefficient constant for enhancement signal	147
Figure 5.23	The coefficient constant for fade signal	148
Figure 5.24	Comparison of the proposed model and the 95% confidence interval of the enhancement signal measured data	150
Figure 5.25	Comparison of the proposed model and the 95% confidence interval of the fade signal measured data	150
Figure A1	Rainfall rate climate regions (Crane, 1980)	169
Figure A2	Rainfall climatic zones of the Earth (CCIR Report 563-4, 1990)	170

Figure A3	Rainfall rate contours for 0.01% of the time for South East Asia (ITU-R P.837-3, 2001)	171
Figure B1	Functional diagram of the RS-102 tipping bucket type rain gauge	172
Figure B2	Top view of the Casella tipping bucket rain gauge	173
Figure B3	Block diagram of beacon receiver used in USM, KMITL, ITB, AdMU and USP	173
Figure C1	Variation of monthly rainfall amount at the measurement site for year 2002	174
Figure C2	Variation of monthly rainfall amount at the measurement site for year 2003	174
Figure C3	Example of rainfall attenuation time series	175
Figure C4	Rainfall rate conversion factor at measurement site for 2 years	175
Figure C5	The confidence limits for the 2 years rainfall rate data	177
Figure C6	The confidence limits for the 2 years rainfall attenuation data	178
Figure C7	Comparison of rainfall rate conversion method with 1-minute measured rainfall rate values at USM for 2 years.	182
Figure C8	Comparison of rainfall rate conversion method with 1-minute measured rainfall rate values at KMITL for 2 years.	183
Figure C9	Comparison of rainfall rate conversion method with 1-minute measured rainfall rate values at USP for 2 years	183
Figure C10	Comparison of rainfall rate conversion method with 1-minute measured rainfall rate values at ITB for 2 years	184
Figure C11	Comparison of rainfall rate conversion method with 1-minute measured rainfall rate values at AdMU for 2 years	184
Figure C12	Comparison of 1-minute rainfall rate prediction models with measured data at USM for 2 years	185
Figure C13	Comparison of 1-minute rainfall rate prediction models with measured data at KMITL for 2 years	186
Figure C14	Comparison of 1-minute rainfall rate prediction models with measured data at USP for 2 years	187
Figure C15	Comparison of 1-minute rainfall rate prediction models with measured data at ITB for 2 years	188
Figure C16	Comparison of 1-minute rainfall rate prediction models with measured data at AdMU for 2 years	189

Figure C17	Comparison of 1-minute rainfall attenuation prediction models with measured data at USM for 2 years	193
Figure C18	Comparison of 1-minute rainfall attenuation prediction models with measured data at KMITL for 2 years	194
Figure C19	Comparison of 1-minute rainfall attenuation prediction models with measured data at USP for 2 years	195
Figure C20	Comparison of 1-minute rainfall attenuation prediction models with measured data at ITB for 2 years	196
Figure C21	Comparison of 1-minute rainfall attenuation prediction models with measured data at AdMU for 2 years	197
Figure C22	Time series of clear sky quantization signal level	203
Figure C23	Example of scintillation observed from beacon on a clear day	203
Figure C24	Comparison of the 2 years measured scintillation enhancement signal amplitude with prediction models.	205
Figure C25	Comparison of the 2 years measured scintillation fade signal amplitude with the prediction models	206
Figure C26	(a) Rainfall rate and rainfall attenuation, (b) wind speed and wind direction and (c) temperature and Humidity during daytime	207
Figure C27	(a) Rainfall rate and rainfall attenuation, (b) wind speed and wind direction and (c) temperature and Humidity during night time	208
Figure C28	Correlation between rainfall attenuation and rainfall rate for 2 years	209
Figure C29	Correlation between wind speed and rainfall rate	209
Figure C30	Correlation between temperature and rainfall rate	209
Figure C31	Correlation between humidity and rainfall rate	210
Figure C32	Correlation between wind speed and rainfall attenuation	210
Figure C33	Correlation between temperature and rainfall attenuation	210
Figure C34	Correlation between humidity and rainfall attenuation	211
Figure C35	Correlation between wind speed and scintillation intensity	211
Figure C36	Correlation between temperature and scintillation intensity	212
Figure C37	Correlation between humidity and scintillation intensity	212
Figure C38	Rainfall rate with different wind speed for 2 years at USM	213
Figure C39	Rainfall attenuation with different wind speed for 2 years at USM	213

## LIST OF SYMBOLS

$A(\theta, \lambda, \rho)_{\text{cloud}}$	cloud attenuation (dB)
$A_{0.01}$	attenuation exceeded for 0.01% of an average year (dB)
$A_p$	attenuation to be exceeded for other percentages of a average year (dB)
$A_s(p)$	scintillation fade depth for the time percentage p
$C_n^2(z)$	the height dependent refractive index structure parameter, $\text{m}^{-2/3}$
$D_a$	physical diameter (m) of the earth-station antenna
$D_{\text{eff}}$	effective antenna diameter from the geometrical diameter (m)
$e_s$	corresponding saturation water vapour pressure (mb)
f	is the operating frequency (GHz)
g(x)	antenna averaging factor
H	average surface relative humidity (%) at the site for a period of one month or longer
$H_e$	is the effective rain height (km)
$h_{\text{fr}}$	freezing height during rain (km)
$H_o$	is the earth station altitude (km)
$h_o$	equivalent height for oxygen
$h_s$	is the height above the mean sea level of the earth station (km)
$h_w$	equivalent height for water vapour
k and $\alpha$	are the regression coefficients for specific attenuation
l	is the horizontal projection of the slant-path
$L_e$	effective path length through rain (km)
$L_g$	horizontal projection of the slant-path length(km)
$L_o$	is the outer scale of turbulence, (m).
$L_r$	adjusted rainy path length
$L_s$	slant-path length below the freezing height(km)
M	is the average annual total rainfall depth, mm

$M(z)$	the vertical radio frequency of the refractive index gradient ( $m^{-1}$ )
$N_{wet}$	'wet term' of the radio refractivity
$P$	is the percentage of time (%)
$P(\chi > \chi_0)$	the cumulative distribution of $\chi$ (%)
$P(Cu)$	the Probability of the Cumulus cloud (%)
$P(R \geq r)$	is the the probability that R exceeds a given rainfall rate $r$ (mm/h) in percentage of time (%)
$P_1$	exceeded yearly time probability (%) for 1-minute of time
$P_0$	is the probability that the rain will fall at the point where the rainfall rate R is measured
$P_t$	exceeded yearly time probability (%) for $t$ (5,10,20,60)-minute of time
$p_t(P)$	is the conversion factor
$R$	rainfall rate (mm/h)
$R_{0.01}$	point rainfall rate for 0.01% of an average year (mm/h)
$R_1(P)$	is the one minute integration time that the rain rate (mm/h) exceeded at a percentage of time P
$R_{60}(P)$	is corresponding 60-minutes integration time rainfall rate (mm/h)
$R_{eff}$	effective antenna radius(m)
$rh_{0.01}$	horizontal path adjustment factor for 0.01% of the time
$R_p$	is the rainfall rate(mm/h) at a certain percentage of time
$R_t(P)$	is corresponding $\tau$ minutes integration time rainfall rate (mm/h)
$t$	average surface ambient temperature ( $^{\circ}C$ ) at the site for a period of one month or longer.
$y_e(P)$	the distribution of signal enhancement (dB)
$y_f(P)$	the distribution of signal fade (dB)
$z$	the height above the ground level, meters

## PEMBINAAN MODEL HUJAN DAN SINTILASI PADA JALUR KU DALAM NEGARA-NEGARA TROPIKAL ASIA TENGGARA

### ABSTRAK

Pengukuran kadar hujan, pelemahan dan sintilasi selama dua telah dijalankan dalam negara-negara Tropikal Asia Tenggara (USM, KMITL, USP, AdMU dan ITB). Data – data yang diperolehi digunakan untuk menyiasat rosotan yang disebabkan oleh hujan pada lintasan satelit yang beroperasi di negara-negara tropik dan khatulistiwa. Taburan longgokkan kadar hujan, pelemahan dan sintilasi yang dihasilkan daripada data yang disukat telah diuji dan dibandingkan dengan model-model ramal yang sediada. Model-model ramalan yang sediada untuk lintasan perambatan tidak menunjukkan persetujuan yang baik dengan data-data yang diperolehi melalui ujikaji. Ini menunjukkan bahawa model hujan perlu dibangunkan untuk negara-negara tropik. Keputusan ujikaji telah dianalisis untuk memahami potensi and penghadan setiap model ramalan. Berdasarkan kepada penghadan model-model yang sediada, model-model kadar hujan dan pelemahan yang baru, telah dibangunkan berdasarkan kepada pengetahuan pada taburan longgok kadar hujan dan pelemahan yang diperolehi daripada kawasan dimana ujikaji dilaksanakan. Perbandingan diantara model ramalan dan keputusan daripada ujikaji telah menunjukkan penambahbaikan yang ketara pada ralat ramalan jika dibandingkan dengan model-model yang sediada. Model yang dicadangkan juga telah digunakan untuk ramalan pada lokasi yang berbeza di Brazil, Singapore dan Papua New Guinea. Model-model yang dicadangkan telah menghasilkan taburan longgok yang baik, dengan ralat rms rendah pada lokasi dimana uijikaji telah dijalankan dan pada lokasi yang berbeza untuk ketiga-tiga kawasan yang dinyatakan diatas. Persetujuan dengan data-data ujikaji didapati bergantung kepada parameter-parameter yang sesuai oleh model-model yang dicadangkan kepada pembolehubah meteorologi radio pada lintasan satelit. Oleh itu boleh disimpulkan bahawa model-model yang dicadangkan mempunyai ketepatan ramalan yang tinggi pada keseluruhan taburan longgokkan untuk data-data hujan dan sintilasi.

## DEVELOPMENT OF RAIN AND SCINTILLATION MODELS AT KU-BAND IN SOUTHEAST ASIA TROPICAL COUNTRIES

### ABSTRACT

A two year rainfall rate, attenuation and scintillation measurement was conducted in Southeast Asia Tropical countries (USM, KMITL, USP, AdMU and ITB). The data obtained are useful to investigate the impairment due to rainfall in satellite links operating in tropical and equatorial climates. The cumulative distributions of rainfall rate, attenuation and scintillation derived from the measured data are presented and compared with those obtained with existing prediction models. Existing model for prediction of slant-path have not shown good agreement with available experimental data, confirming the need of suitable models for tropical region. Results were analysed in order to understand the potentials and the limits of each prediction model. Based on the limitations of the existing models, 1-minute rainfall rate and attenuation prediction model was developed from the knowledge of the ground point rainfall rate and attenuation cumulative distribution representative of the area where the earth station is located. Comparison between predicted and experimental results has shown significant improvements in terms of reduced prediction error over existing models. The proposed models were also used for prediction against the measured data from different location such as Brazil, Singapore and Papua New Guinea. The proposed model gave a good representation of cumulative distribution with an overall low rms for measurement sites and the three different locations mentioned above. The agreement with the measured data was found to be mainly dependent on the proper parameterization of the proposed models to the radiometeorological variables along the satellite link. Therefore, it can be concluded that the proposed models has high prediction accuracy for the whole cumulative distribution of rainfall and scintillation data.

## CHAPTER 1

### INTRODUCTION

#### 1.1 Background

The rapid growth of satellite services using higher frequency bands such as the Ku-band have highlighted a need for estimating the combined effect of different propagation impairments. However, the effects of the earth's atmosphere on radiowaves propagating between earth and space platforms are a constant concern in the design and performance of space communication systems. The problem becomes more serious for systems operating above 10 GHz, where the radiowave link can be adversely affected by precipitation, atmospheric gases (primarily oxygen and water vapor) and tropospheric scintillation. These propagation impairments are more critical in tropical and equatorial zones compared to temperate zones (Dissanayake *et al.*, 1997; Karasawa *et al.* 1988; Mouldsley and Vilar, 1982; Crane, 1980).

Attenuation that is caused by rain and scintillation will affect a particular communication system in terms of signal losses and be temporarily unavailable for use. This phenomenon is known as outage time where the amount of time during which the satellite system performance will be below the design threshold value and it will not be usable. Therefore to overcome this problem one- minute rainfall rate, attenuation and scintillation need to be studied and used to calculate the expected amount of rainfall attenuation and scintillation attenuation to prevent the unavailability or outage time from occurring (Crane, 1996, Ajayi, 1996a, CCIR Study Group, (1986-1990)).

When considering parameters affected by propagation impairments factor, it is necessary to specify the parameters on a statistical basis, which are usually specified in percentage of time. This percentage of time is normally described as the percentage of time in a month, in a year or the parameter equals to or exceeds a certain value so

that the link margin can be established. Link margin is the additional transmitter power required to overcome the signal fade.

Accurate rainfall measurement in tropical and equatorial regions has long been and remains a difficult task(Crane, 2003). There are also some parts in this region where the prime rainfall data cannot be obtained or not available to calculate the cumulative one-minute rainfall rate distribution. Therefore prediction models are required to predict the local cumulative distribution of one-minute rainfall rate. Many researchers have developed models that can be used to estimate one-minute rainfall rate distributions. These models derived by many can be classified in two ways. The first method, Crane (1996) and ITU-R P.618-7 (2001) divided the world into twelve regions with different rainfall rate values for each region. The second method specific climatic data are required to calculate the rainfall rate. Those models are Moupfouma (1995), Lognormal (Morita,1980) and Dutton&Dougherty (1978). Most of this rainfall rate models were developed based on the rainfall data collected in temperate regions such as Lognormal (Morita,1980), Gamma (Morita, 1971) , Stutzman and Dishman (1986) and very few in tropical and equatorial such as Moupfouma (1995), ITU-R P.618-7(2001) and Crane(1986).

Unfortunately not all countries have one-minute rainfall rate data. Therefore an hourly rain accumulation data collected by meteorological institutes are available in these countries that can be used for analysis (Pontes, 1990). A conversion method is required to convert higher integration time statistics (sixty-minute) to equivalent one-minute rainfall distribution. This conversion method has been proposed by Segal (1986), which was adopted by CCIR Study Group(1986-1990), Burgueno (1988), Chebil and Rahman (1999) and Hwan (2002). This method was also studied and calculated for the measured locations and compared them with the one-minute rainfall rate cumulative distribution at each of these locations.

The reason why sixty minutes rainfall data must be converted into one-minute rainfall rate is because the one-minute rainfall rate knowledge is very important in order to calculate the rainfall attenuation at a specific location (Chebil and Rahman, 1999). More over, the evaluation of the effects of rain on satellite system design requires a detailed knowledge of the attenuation statistics for each ground terminal location at the specific frequency of interest (Crane, 2003). Direct long-term measurement of rainfall attenuation for all of the ground terminal locations in an operational network are not practical, therefore modeling and prediction methods must be used to make an estimate of the expected attenuation for each location. More over, rainfall attenuation predictions are generally required for locations different from the limited number of stations with sufficient long-term data for the preparation of a statistically reliable distribution estimate.

Rainfall attenuation can be directly obtained from the measurement of radiometer or beacon receiver (Dissanayake *et al.*, 1990 ; Juy *et al.*, 1990; Pan and Bryant, 1992; Matricciani, 1993; Ong and Zhu, 1997) or predicted from the drop-size distribution or knowledge of rainfall rate (Crane, 1996). The method for predicting the attenuation is based on the relationship between the specific attenuation and rainfall rate established through the modeling of the rain shape, rain size, temperature and terminal speed of the raindrops. The rain induced attenuation is computed by integrating the specific attenuation along the propagation path (Ajayi, 1996a). The calculation of the specific attenuation requires a cumulative distribution of rainfall rate that is one-minute integration of time (Leitao & Watson, 1986). Therefore one-minute rainfall rate cumulative distribution plays an important role in calculating the rainfall attenuation distribution. For locations where essential one-minute rainfall rate distribution cannot be obtained, predictions models are required to predict the local cumulative distribution of one-minute rainfall attenuation.

Over the past several years extensive efforts have been undertaken to develop reliable (where the models will have a RMS percentage error below 10%, ITU-R P.618-7, 2001) techniques for the prediction of path rain attenuation for a given location and frequency, and the availability of satellite beacon measurements have provided a database for the validation and refinement of the predictions models. Most of this rainfall attenuation model that has been developed by researches were based on the data collected from temperate regions such as Lin (1981), Stutzman and Dishman (1986) and Crane (1980) where else ITU-R P.618-7 (2001) and Dissanayake (1997) models are based on global data collection. This rainfall attenuation prediction models were studied, calculated and compared with the prime rainfall attenuation data obtained from the measured locations. The accuracy (the degree of conformity of a measured or calculated value to its actual or specified value) of a model depends on the applicability of the database for the location of interest.

Besides rainfall rate and attenuation, scintillation also plays an important role in signal degradation on a satellite link. Therefore, in the past few years many microwave propagation experiments have been carried out to evaluate the impact of tropospheric scintillations on the budget design of satellite link (Moulsley and Vilar, 1982; Geoffroy *et al.*, 1997; Karasawa *et al.*, 1988 ; Kamp, 1998; Otung *et al*, 2003). These experiments usually involve large resources and are generally not easy to set up for each link. To cope with these problems, there has been a growing interest in developing statistical methods (models used to calculate the scintillation intensity at different percentage of time) for predicting tropospheric scintillation directly from meteorological data. On the other hand, these prediction models can be based on experimental data of a collection of beacon sites whose results are generally extended to other sites and frequencies by means of empirical functions (Karasawa, Yamada and Allnutt, 1988; Ortigies, 1993; Merlo, Fionda and Wang, 1988).

Knowledge of the distribution scintillation intensities can be used to achieve an expression for long-term probability distribution of scintillation amplitude fluctuation, which permits a detailed evaluation of the availability of a satellite link (Otung *et al.*, 1995). Several prediction models of one-minute scintillation intensity cumulative distribution and probability distribution function (PDF) were developed by researches to predictive the one-minute scintillation intensity. Each prediction model is studied in order to understand the type of the input requirements. Tropospheric scintillation models were mostly developed based on scintillation intensity collected in temperate climate such as ITU-R P.618-7 (2001), Karasawa (1988), Otung (1996), Ortigies (1993) and many others by combining theoretical relations and experimentally observed dependencies (Matricciani *et al.*, 1997; Salonen *et al.*, 1996; Vilar and Haddon, 1984; Catalan and Vilar, 2002; Kassainides and Otung, 2003). The evaluation and comparison of some of these statistical models for the monthly prediction of clear-air scintillation amplitude from ground meteorological measurement were done in USM (100.4°E 5.17°N).

Measurement of rainfall rate (one-minute and sixty-minute) and rainfall attenuation were done in five locations of tropical and equatorial countries, Malaysia (Universiti Sains Malaysia (USM), 100.4°E 5.17°N), (Indonesia Insitute Teknologi Bandung (ITB), 107.4°E 6.5°S), Thailand (King Mongkut's Institute of Technology Ladkrabang (KMITL), 100.8°E 13.7°N), Philippines (Ateneo de Manila University (ADMU), 121.1°E 14.7°N) and Fiji (University of South Pacific (USP), 178.5°E 18.1°S). This system consists of one set of fast tipping bucket-type rain gauges (0.5 mm tipping bucket), data micrologger, a central computer and a satellite beacon receiver. The collected rainfall data and meteorological data from various instruments for these five locations were converted into real time data by a computer software that was installed by Post-PARTNERS (Pan pacific Regional Telecommunication Network Experiment

and Research by Satellite Japan) named 'Kisyo'. 'Kisyo' is a data acquisitions and logger program.

## **1.2 Objectives of the Research**

The objectives of this thesis are: -

- a. To make comparisons of the measured rainfall rate, attenuation and scintillation data with the existing propagation models.
- b. To develop a rainfall rate, attenuation and scintillation model based on direct measurement data obtained from USM, KMITL, USP, AdMU and ITB.
- c. To perform statistical analysis of rainfall rate, attenuation and scintillation data.

## **1.3 Organization of the Thesis**

The report is organized in chapters whereby Chapter 1 introduces the importance of rainfall rate, attenuation and scintillation research in order to establish a reliable satellite communication link in the tropical and equatorial regions. This chapter also describes the work done by other researchers in deriving at the many rain and scintillation models. Chapter 2 describes the theory of rainfall rate, attenuation and scintillation measurements that are used in deriving rain and scintillation models. The rainfall rate conversion models, one-minute rainfall rate models, rainfall attenuation models and scintillation models are explained.

Chapter 3 describes the set up of the rainfall and beacon signal data collection system. The operation of the tipping bucket rain gauge and the beacon receiver are explained. The calibration of the instruments used, the type of measurement errors accounted for, and the measurement errors obtained from the measurement sites are stated.

Chapter 4 presents the analysis and results of the propagation research in USM, KMITL, USP, ITB and AdMU. The confidence level of the measured data is calculated by the given equation and the confidence intervals of the measured data are shown in the graphs. A 95% confidence interval was used to find out whether the pre-existing models predicted values lie in between the confidence intervals of the measured data. The models were also compared in terms of percentage errors and Real Mean Square (RMS) values. The effects of wind speed, temperature and humidity are also considered towards the rainfall and scintillation data.

Chapter 5 presents the development of rain and scintillation models. The developed models are compared with the measured data in terms of percentage errors and RMS values. A 95% confidence interval was used for the measured data to find out whether the derived models predicted values lie in between the confidence interval of the measured data. The derived models were used for prediction at different measurement site, to find whether the data form different measurement sites lie in between the 95% confidence interval of the derived models values for the entire measurement time.

Chapter 6 concludes by summarizing the results of the statistical analysis done for the data collected and the developed models. Some recommendations for future work are also proposed.

## CHAPTER 2

### RAINFALL AND SCINTILLATION MODELS

#### 2.1 Introduction

Rainfall attenuation is by far the most important of losses for frequencies above 10GHz, because it can cause the largest attenuation and is usually, therefore, the limiting factor in Ku band satellite link design (Timothy *et al*, 2003). Rainfall rate distribution is one of the most important factors for calculating rainfall attenuation at a specific location. The most effective way of obtaining the cumulative rainfall distribution is through direct measurement. However due to the shortage of the required rainfall data at certain locations, rainfall models need to be introduced to predict the rainfall rate and attenuation distribution at location of interest (Mandeep and Hassan, 2003; Panagopoulus and Kanellopoulus, 2003; Ahmad *et al*; 2004).

Another signal degradation factor for frequency above 10 GHz is tropospheric scintillation. At millimeter-wave frequencies, scintillation may seriously affect satellite-earth links where it yields random fades and enhancements of the received signal particularly at low elevation angles. Therefore, accurate estimates of signal degradation due to this effect must be included in the design of satellite communication systems (Mandeep *et al*, 2004).

This chapter reviews rainfall and scintillation models that will be used in calculating the cumulative distribution of the models. The main objective is to evaluate and compare some statistical models for the annually prediction rainfall and scintillation from ground meteorological measurements.

## 2.2 The Importance of Rainfall Rate

The rainfall rate,  $R$  is defined as the volume of liquid water that falls through a unit area per unit time and is normally expressed in unit millimeters per hour (mm/h) (Olsen *et al.*, 1978). Rainfall rate is measured by rain gauge, the most common of which is a tipping bucket. The long-term behavior of rainfall rate is described by a cumulative probability distribution or by a cumulative distribution function (cdf). The cdf for rainfall rate is commonly referred to as an exceedance curve. This gives the percentage of time (usually the percentage of 1 year) that the rainfall rate exceeds a given value (Timothy *et al*, 2003).

Rain affects the design of any communication system that depends on the propagation of radiowave signal through the lowest 10km of earth's atmosphere at frequencies above 10GHz. Satellite systems or in brief communication system may experience a loss of radiowave signal due to the attenuation caused by rain (Kumar and Ramachandran, 2004; Matricciani, 2000; Matricciani and Riva, 2003). Scattering by rain introduces interfering signals into satellite system will cause the original signal to degrade and mask the desired signal (Lin, 1974, Crane, 1980).

One –minute rainfall rate statistics are required to setup a communication link. More than estimate of the surface point rainfall rate distribution is required for the prediction of attenuation on terrestrial or earth to space (Crane, 1980). Rain displays significant spatial and temporal variation along a horizontal path, and procedures are required to statistically estimate the instantaneous rainfall rate along the path. There is no physical theory that exists to calculate the surface point rainfall rate distribution (Crane, 2003). The distribution of rainfall rate is empirical and must be developed from available long-term observation of rain accumulation.

Beside of direct rainfall rate measurement, predictions model for rainfall rate are required for locations different from the limited number of stations or locations with sufficient long-term data for the preparation of a statistically reliable distribution estimate (Rice and Holmberg. 1973; Alasseur *et.al.*, 2004).

Researchers such as Feldhake and Sengers (2002), Migliora *et.al* (2003), Miranda *et al.* (1997), Yamada *et al.* (1987), Joo *et al.* (2002), Chebil *et al.* (1995), Paulson and Gibbins (2000), Pontes *et al.* (2003) and Ong (1997) has mentioned that long term rainfall data allows to make good statistical analysis measurement and comparison of the pre-existing rainfall models. Even though with the absent of long term data, these researches has compared pre-existing rainfall models with short term (2 years) measured rainfall data and proved that there were models that allow to make good prediction.

### **2.3 Rainfall in Tropical and Equatorial Regions**

In the tropical and equatorial region, meteorologists have classified rain precipitation in two categories (Ajayi *et al*, 1996a, Timotty *et al*, 2003; Ramachandran and Kumar, 2004). Stratiform rain is generated in cloud layers containing ice, and results in widespread rain at rainfall rates less than 10 mm per hour.

Convective rain is generated by the vertical air currents that can be very powerful, leading to thunderstorms and high rainfall rates. Convective rain is very important for satellite communication systems because it is the major cause of link outage. Stratiform rain consists of a generally constant rainfall rate over a very large area while convective rain is generally confined to a narrow, but tall, column of rain. Figure 2.1 and Figure 2.2 shows the two phenomena.

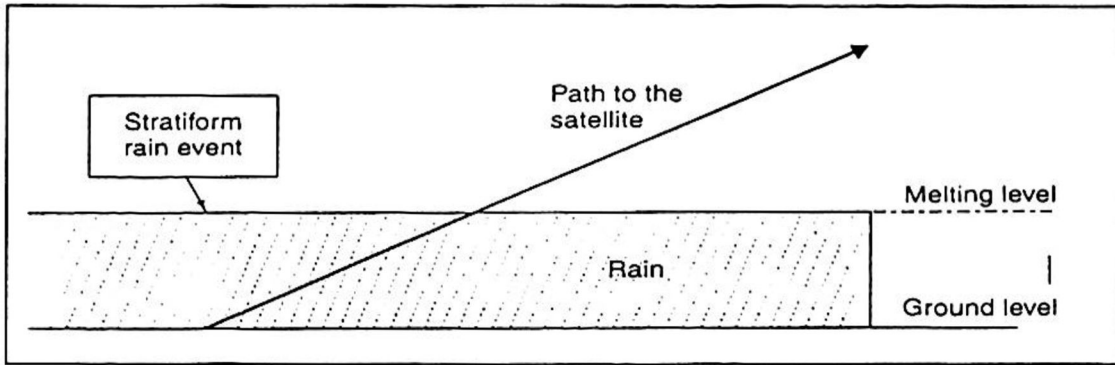


Figure 2.1 Stratiform rainfall situations

Figure 2.1, shows that the widespread system of stratiform rain completely covers the path to the satellite from the ground up to the melting layer. Stratiform rain occurs typically ahead of warm front in an area of low pressure. Large areas of cloud exists in which ice crystals are sufficiently large to slowly fall and join other ice crystals to form snowflakes, which fall more quickly as their size increases.

If there is a high concentration of moisture in the clouds, in the form of ice, large snowflakes may form. The snow falls until it reaches the melting layer. The melting layer is simply the region of the atmosphere where the temperature transitions from below  $0^{\circ}\text{C}$  to above  $0^{\circ}\text{C}$ . Snow falling into air temperature greater than  $0^{\circ}\text{C}$  melts and forms raindrops. This leads to generally constant attenuation of the slant-path signals over the entire path length from the ground to the melting layer (Timothy *et al*, 2003).

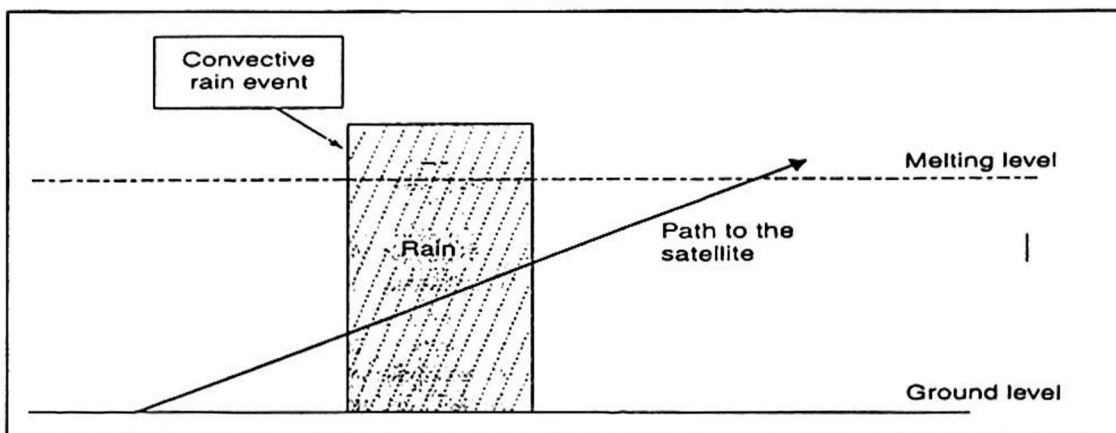


Figure 2.2 Convective rainfall situations

In Figure 2.2 the tall column of convective rains enters the satellite to ground path. In some cases storm will be in front of the earth station and in other times behind it. Convective rainstorms are very complex and have both horizontal and vertical structures. A convective cell becomes established when a mass of warm moist air is pushed up into colder air at higher altitude. Adiabatic expansion of the air mass occurs, which cools the air. When the air is cooled below its dew point, it condenses forming clouds and drops of water start to fall under gravity. The falling drops collide and coalesce with other drops to make larger drops, leading a drop size distribution.

#### 2.4 Prediction of Rainfall Attenuation using Rainfall Rate

A fundamental quantity in the calculation of rain attenuation statistics for terrestrial and earth space paths is the specific attenuation  $\alpha$  or attenuation per unit distance. Specific attenuation has been calculated by two approaches which are theoretical method employing a uniformly random distribution of raindrops modeled as water sphere or more complex shapes and an empirical procedure based on the approximate relation between  $\alpha$  and the rain rate  $R$ , (Olsen & Rogers, 1978; Maekawa *et al.* 2004).

The specific attenuation is given as

$$\alpha \text{ (dB/km)} = aR^b \quad (2.1)$$

where  $a$  and  $b$  are functions of frequency  $f$  and the average rain temperature  $T$ . The coefficient  $b$  was taken to be unity (Ryde, 1946). After that Olsen *et al* (1978) calculated the value for  $a$  and  $b$  from Marshall and Plamer (1948), Laws and Parsons (1943) and Joss *et al* (1968) dropsize distribution at various temperatures of  $-10$ ,  $0$  and  $20^\circ$  Celsius for frequencies between  $1$  and  $1000$  GHz.

Then CCIR adopted and reproduced (CCIR report 721, 1986) for frequencies ranging from  $1$  to  $400$  GHz. CCIR replaced  $a$  with  $k$  and  $b$  with  $\alpha$ , and the specific

attenuation  $\alpha$  with  $\gamma$  (Allnutt, 1989). Table 2.1 shows the value for  $k$  and  $\alpha$  at a temperature of 20° Celsius by using the Laws and Parsons dropsize distribution, Gunn and Kinzer (1949) terminal velocity of raindrops, Ray (1972) refractive index of water and Fedi (1979) and Maggoiri (1981) regression analyses.

Attenuation by rain can be predicted accurately if the rain is precisely described all the way along the path. Path attenuation is essentially an integral of all individual increments of rain attenuation caused by the drops encountered along the path (Maitra, 2004; Matricciani, 2004; Kumar, 2004). This is physical approach to predict rain attenuation. Unfortunately, rain cannot be described accurately along the path without extensive meteorological database, which does not exist in most regions of the world (Timothy *et al*, 2003). Most prediction models therefore resort to semi empirical approaches.

The semi empirical approach is based on two factors, firstly the rainfall rate at a point on the surface of the earth is statically related (over a period of at least a year) to the attenuation encountered along the path to a satellite and secondly the actual path length of the path through the rain medium can be adjusted in such a way that the *effective path length*,  $L_{eff}$  is developed over which the rain can be considered to be homogeneous.

The effective path length is defined by CCIR Report 563-4 (1990) as the length of hypothetical path obtained dividing the total rain attenuation over the path by the specific attenuation measured at the ground and exceeded for the same percentage of time. Thus the equation is written as,

$$A(\text{dB}) = kR^\alpha L_{eff} \quad \text{dB} \quad (2.2)$$

where

$$L_{\text{eff}} = r_p \cdot L \quad (2.3)$$

L is the actual path length, km and  $r_p$  is the reduction factor. The  $r_p$  depends on the spatial distribution of rainfall rate and accounts horizontal variations of the rain along a path. The purpose of the reduction factor is reducing the point rainfall rate to the path averaged rainfall rate or to reduce the actual path length filled with uniform point of rainfall.

Table 2.1 Regression coefficients for estimating specific attenuation in equation (2.1). (Recommendation ITU-R P.838-1, 2001).

Frequency (GHz)	$k_H$	$k_V$	$\alpha_H$	$\alpha_V$
1	0.000387	0.000352	0.912	0.880
2	0.000154	0.000138	0.963	0.923
4	0.000650	0.000591	1.121	1.075
6	0.00175	0.00155	1.308	1.265
7	0.00301	0.00265	1.332	1.312
8	0.00454	0.00395	1.327	1.310
10	0.0101	0.00887	1.276	1.264
12	0.0188	0.0168	1.217	1.200
15	0.0367	0.0335	1.154	1.128
20	0.0751	0.0691	1.099	1.065
25	0.124	0.113	1.061	1.030
30	0.187	0.167	1.021	1.000
35	0.263	0.233	0.979	0.963
40	0.350	0.310	0.939	0.929
45	0.442	0.393	0.903	0.897
50	0.536	0.479	0.873	0.868
60	0.707	0.642	0.826	0.824
70	0.851	0.784	0.793	0.793
80	0.975	0.906	0.769	0.769
90	1.06	0.999	0.753	0.754
100	1.12	1.06	0.743	0.744
120	1.18	1.13	0.731	0.732
150	1.31	1.27	0.710	0.711
200	1.45	1.42	0.689	0.690
300	1.36	1.35	0.688	0.689
400	1.32	1.31	0.683	0.684

#### 2.4.1 Prediction of Rainfall Attenuation using Equiprobability Method

There is usually no relationship between simultaneous values of the attenuation  $A(\text{dB})$  and the point rainfall rate  $R(\text{mm/h})$  measured on the ground near a receiving

antenna.. This is because raindrops (usually caught in updrafts) require a long time to fall from upper part of a storm to a ground-based rain gauge (Perez, 2004; Khajepiri *et. al*, 2004). Typically the behavior of the attenuation at time  $t$  resembles the behavior of the ground rain rate of time  $(t + T)$  where  $T$  is the delay and may be as long as 4 to 8 min. This is why predictive models for rainfall attenuation are statistical rather than instantaneous (Pratt & Bostian, 1986).

Figure 2.3 illustrates the procedure for finding equiprobable values of rainfall rate and rainfall attenuation. For a given time  $P$ , the rainfall rate is read off the rainfall rate statistics and the rainfall attenuation is read off the rainfall attenuation statistics. For example at  $P\%$  of time, from Figure 2.3(a) the rainfall rate is read off as  $R(P)$  mm/h and from Figure 2.3(b) the rainfall attenuation is read off as  $A(P)$  dB.  $R(P)$  and  $A(P)$  are rainfall values for example,  $R(P)$  could be 97 mm/h and  $A(P)$  could be 17 dB.

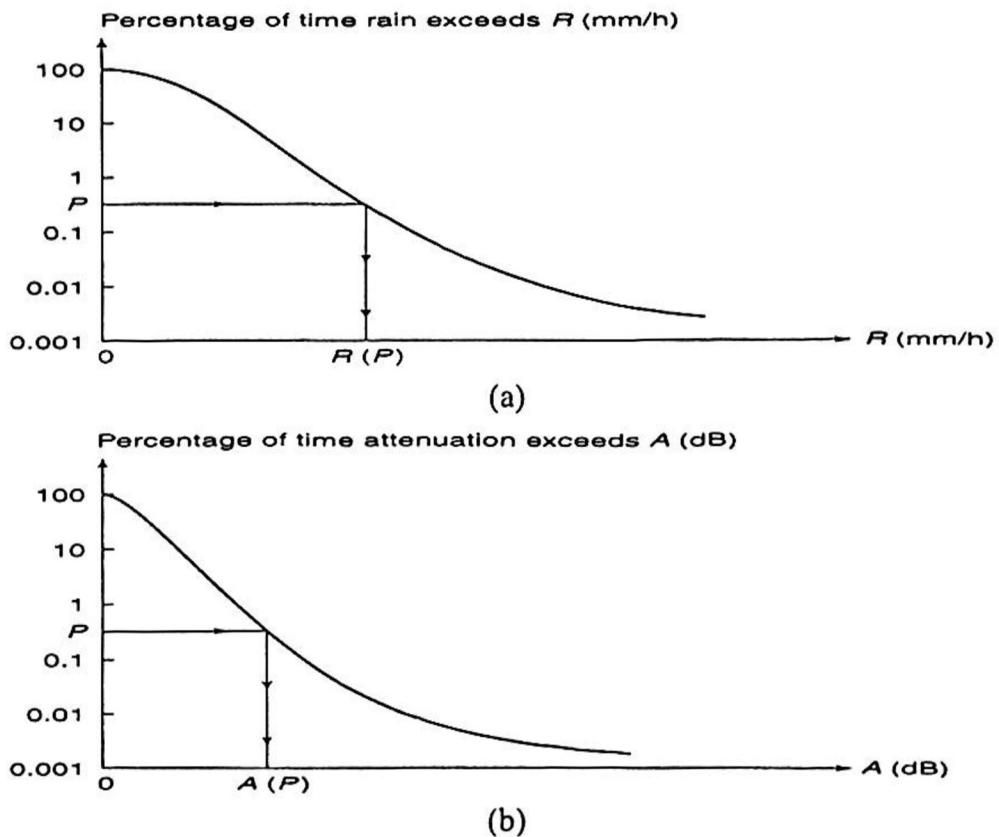


Figure 2.3 Procedure for finding equal-probability value of rainfall rate,  $R$  and attenuation,  $A$ .

Attenuation and rainfall rate values so paired are called *equal-probability values*. The disadvantage of this approach is outweighed by the improved accuracy obtained by extrapolating to both low and high time percentages, where the rainfall rate measurements are somewhat suspect (Timothy *et al.*, 2003).

## 2.5 Prediction of Tropospheric Scintillation

Predicting tropospheric scintillation became a growing interest by many researchers to develop statistical methods based directly from meteorological data (Karasawa *et al.*, 1988, Mousley and Vilar, 1982, Ortgies, 1993, Tervonen *et al.*, 1998, ITU P.618-7, 2001). This prediction model can be based on experimental data from a collection of beacon sites whose results are generally extended to others sites and frequencies by means of empirical functions (Geoffroy *et al.*, 1997).

### 2.5.1 Theory of Tropospheric Scintillation

The atmosphere that is close to the ground is sometimes called the boundary layer and its rarely still. Energy from the sun warms the surface of the earth and the resultant convective activity disturbs or agitates the boundary layer. This agitation results in turbulent mixing of different parts of the boundary layer, causing small-scale variations in the refractive index. Figure 2.4 shows the turbulence process (Timothy *et al.*, 2003)

Figure 2.4(a) shows the stratified layers (calm conditions). The air is calm and the lower atmosphere next to the earth's surface (the boundary layer) forms into layers. Each layer has a slightly different refractive index, decreasing in general with height. Figure 2.4(b) shows the turbulent mixing (convective conditions). In this figure, the earth's surface has become heated by energy from the sun and the resultant convective activity has mixed the formerly stratified layers into 'bubbles' that have different refractive indices.



Figure 2.4 Schematic of stratified and turbulent conditions in boundary layer of the atmosphere.

When the signal encounters a turbulent atmosphere, the rapid variations in the refractive index along the path will lead to fluctuations in the received signal level. These fluctuations are generally fairly constant around the mean signal level and are called *scintillation*. Tropospheric scintillation is caused by rapid fluctuations in the amplitude of the received signal arising from the random fluctuations in the atmospheric refractive index due to turbulent irregularities. (Timothy *et al.*, 2003, Savvaris, 2004).

### 2.5.2 Theory of Turbulence-Induced Scintillation

Tatarski introduced a theoretical formulation for the estimation of log-amplitude fluctuations based on the assumption that the spatial structure of the atmospheric refractive index is in accordance with a Kolmogorov-type spectrum (Ishimaru, 1978). When the atmospheric turbulence lies in the inertial sub range of a relation  $r_{\min}^2/\lambda \leq L \leq r_{\max}^2/\lambda$ , then the variance  $\sigma_x^2$  of log-amplitude in dB is given as

$$\sigma_x^2 = 42.48 k^{7/6} [(\sin\theta)^{11/6}] \int_0^L C_n^2(z) z^{5/6} dz dB^2 \quad (2.4)$$

where

$$k(m^{-1}) = 2\pi/\lambda \quad (2.5)$$

with

$l_{\min}$  inner scale of the refractive index irregularities

$l_{\max}$  outer scale of the refractive index irregularities

$L$  is the effective path length between the boundary of turbulence and reception point.

$\lambda$  the wavelength, meters

$\theta$  the elevation angle, degree

$z$  the height above the ground level, meters

$C_n^2(z)$  the height dependent refractive index structure parameter,  $m^{-2/3}$

Several hypotheses have been assumed for deriving the theoretical relationship in equation 2.4. The major assumptions are as follows (Ishimaru, 1978; Vasseur, 1999)

- 1) Turbulence is considered to be well developed so that it satisfies the Kolmogorov theory (where the theory states that in a turbulent layer the kinetic energy is transferred from large scale turbulence to small scale turbulence having an isotropic motion. The breaking up of the energy will eventually stop and will be dissipated into heat by viscous friction) of turbulence where

$$C_n^2(z) = aM(z)^2 L_o^{4/3} \quad m^{-2/3} \quad (2.6)$$

Where  $a \approx 2.8$  is dimensionless constant,  $M(z) = dn(z) / dz$  is the vertical radio frequency of the refractive index gradient ( $m^{-1}$ ) and  $L_o$  is the outer scale of turbulence, (m).

- 2) The incident wave in the turbulent medium is supposed to be a plane wave
- 3) Scintillation is assumed to be weak so that a smooth perturbation method is used to determine the effect of the refractive index inhomogeneities on the wave propagation.

- 4) Equation (2.6) actually consists of the asymptotic approximation of a much more complicated relationship valid for  $L_o \geq \sqrt{\lambda (z / \sin \theta)}$
- 5) Scintillation variance as calculated from (2.4) characterizes the fluctuations of the signal received by a hypothetical point receiver. The finite aperture of an actual receiving antenna creates an integrating or smoothing effect that leads to a reduction of the scintillation variance.

### 2.5.3 Description of Scintillation Effects

Tropospheric scintillation is characterized by two main parameters.

- 1) The log-amplitude  $\chi$  (in decibels); that is, the ratio of the instantaneous amplitude of the observed signal to the mean amplitude, expressed in decibels (dB). The mean amplitude is generally calculated by a 60-s moving average filter (cutoff frequency around 0.01 Hz) (Vasseur, 1999) in order to separate rapid turbulence induced scintillation from spacecraft-induced variations and contributions of other propagation factors
- 2) The scintillation variance,  $\sigma^2$  in dB<sup>2</sup>; that is, the variance of the log-amplitude  $\chi$ . In order to produce a good estimator of the instantaneous scintillation effect and accounting for its time-variability, the variance is generally calculated in sliding way over about one minute.

Because the turbulence-induced scintillation is a very complicated process, it is important to assess its statistical features. It appears that a scintillation event is characterized by a stationary period of few minutes (up to ten or fifteen minutes). Within this period, the scintillation intensity remains approximately constant and the scintillation log-amplitude distribution can be fitted quite well by a zero-mean Gaussian distribution, whose scintillation intensity is the mean scintillation intensity during the

period (Mandeep *et al*, 2004). For a period longer than several minutes, the variability of  $\sigma$ , must be taken into account and the long-term probability density function (PDF) of the scintillation amplitude can be modeled by a Gaussian distribution with log-normally distributed scintillation intensity (Moulsley and Vilar, 1982; Karasawa *et al*, 1988). The cumulative distribution  $P(\chi > \chi_0)$  of  $\chi$  can be written as (Geoffroy *et al*, 1997)

$$P(\chi > \chi_0) = \int_{\chi_0}^{\infty} \int_0^{\infty} p(\chi|\sigma_\chi) \cdot p(\sigma_\chi) d\sigma_\chi d\chi \quad (2.7)$$

The short term PDF of  $\chi$  follows a Gaussian distribution is written as

$$p(\chi|\sigma_\chi) = 1/(\sqrt{2\pi} \sigma_\chi) \exp (-\chi^2 / (2\sigma_\chi^2)) \quad (2.8)$$

The long term PDF that is log-normally distributed is given by

$$p(\sigma_\chi) = 1/(\sqrt{2\pi} \sigma_\chi s) \exp \{-[\ln(\sigma_\chi^2/m)]^2 / (2s^2)\} \quad (2.9)$$

where  $\chi_0$  is a given threshold value,  $m$  is the median value of scintillation intensity distribution,  $\sigma_\chi$  in dB and  $s$  is the standard deviation of  $\ln(\sigma_\chi^2)$

Most of the statistical models usually try to link the parameters of this PDF to ground meteorological measurements, such as temperature, relative humidity and wind velocity.

The next session reviews several of the rainfall and scintillation models that will be used for comparison with the measured data. All of the rainfall models except for Ong Choo, CETUC, SAM, Joo, Segal and Flavin models were based on data sets used to develop the models by indirect measurements. The rainfall rate observations were not adjusted for gauge integration of time for the possible existence of non-integral year observation periods. In the collection of data, no information's were available about the calibration or dynamic range of the gauges or of the procedure used to adjust for missing data. The majority of the data employed in the generation of the rainfall models

were obtained by meteorological service personnel. In many instances, the rainfall rate observations in the database were obtained as an adjunct to the more important path attenuation measurements and were not subject to strict data quality controls. Given that the attenuation prediction procedures employing the model rainfall rate cumulative distribution function (cdf) works better than prediction procedures for the measured rainfall rate cdfs, it must be assumed that significant rainfall rate sampling errors and measurement errors are present in the data sets.

As for the climatic zones (ITU, Crane, Douglas and Sims) used in equatorial region should be subdivided. A problem arises in that only a very limited number of measured rainfall rate datasets are available in the equatorial region and a further subdivision in the climate zones will negate the main reason for using the climate zone concept. This is the identification of a region with similar rainfall rate characteristics so the available cdfs can be combined to provide statistically stable estimates of the cdf.

## **2.6 Conversion of Rainfall Rate from Sixty-minutes to One-minute**

Methods of using hourly rainfall data for prediction of short duration falls have been sought out by several researches and these methods are empirical or semi-empirical, in that they make use of known properties of the statistics of extreme values (Watson *et al*, 1982). The models that have been developed such as Moupfouma (1995), Segal (1986), Joo (2002), Burgueno (1988) and Chebil and Rahman (1999) takes rainfall data and if necessary any other climatological data and applies one method of conversion, making no adjustment in the empirical parameters on a regional basis. These models are presented below.

### **2.6.1 Segal's Method**

Based on the data analysis from 45 locations in Canada, Segal(1986) proposed a rainfall rate conversion factor where the method is currently adopted by CCIR Report

563-3 (1990). The locations were deliberately chosen to offer a fair sampling of different climatological and physio-graphical regimes. The differences in the quality as well as quantity of rainfall for 10 well-defined rain rate climate zones in Canada were considered. The model was subjectively evaluated by estimating rates at independent locations representing a wide variety of the earth's climates.

Segal, attempted to characterize the differences among the rainfall rate distribution for each climatic zone by means of simple reduction factors relating, for two integration times. The records were derived from approximately ten years of high-resolution daily tipping-bucket rain gauge having integration time of five minutes. The maximum rainfall rate used for deriving Segal's method was 100 mm/h at 0.01 percentage of time. The model gave an RMS percentage error below 10% when applied in Tropical climate. (Segal, 1986). The equation is described as

$$R_1(P) = aP^b R_\tau(P) \quad \text{mm/h (Segal, 1986)} \quad (2.10)$$

where

$p_\tau(P)$  is the conversion factor

$R_1(P)$  is the one minute integration time that the rain rate (mm/h) exceeded at a percentage of time P

$R_\tau(P)$  is corresponding  $\tau$  minutes integration time rainfall rate (mm/h)

a and b are the regression coefficients obtained from the measured data

$\tau$  is the integration time in minutes

### 2.6.2 Burgueno's Method

Using the Spain rainfall database, cumulative distributions were produced on the basis of different effective gauge sampling intervals. The ratios of rainfall rates for different integration times were then analyzed and attempts were made to group the data by geographic location, by climatic zone, and both. Snowfall, which may represent

a substantial fraction of the total annual precipitation at some sites, was not included among any of the measurement data. The model strongly depends on the coefficient  $a$  and  $b$  of the measured rainfall rate data for a particular location. Without the measured data this model cannot be used for conversion. The maximum rainfall rate used for deriving this model at 0.01% of time was 85 mm/h. The model gave a RMS error of 7% when tested in Tropical region.(Silva, *et al.*,1990). The equation is described as

$$R_1(P) = aR_r^b(P) \quad \text{mm/h (Burgueno, et al, 1988)} \quad (2.11)$$

### 2.6.3 Chebil and Rahman's Method

This empirical (Chebil and Rahman, 1999) was proposed for approximating the rainfall rate conversion factor from hourly to 1-minute integration of time for 82 locations in the Malaysian region (Chebil and Rahman, 1999). Chebil and Rahman used the Segal method, which was later modified to produce a better result.

This model depends on the regression coefficient values that are obtained from the measurement site. Differences in the morphology of rainstorms in different parts of the country produced differences in the apparent rain gauge response with respect to integration time. As result, Chebil did not consider a single conversion procedure, where the power law and exponential equation were combined for predictions. The model was formulated to explore a prediction procedure that differs significantly from most of the accepted models for the duration statistics for rainfall events. The maximum rainfall rate that was used to develop this model at 0.01% of time was 145 mm/h. The model gave a RMS error below 5% in UM and UTM (Chebil and Rahman, 1999). The proposed revised model is given as:

$$R_1(P) = R_{60}(P) [aP^{-b} + c \exp (d*P)] \text{ mm/h (Chebil and Rahman, 1999)} \quad (2.12)$$

where

$R_{60}(P)$  is corresponding 60-minutes integration time rainfall rate (mm/h)

a, b, c and d are regression coefficients

#### 2.6.4 Joo's Method

Joo's conversion method (Joo *et al*, 2002) is based on 2 years rainfall rate direct measurement conducted in Korea with the distributions of rainfall rate with 1-, 10-, 20-, 30-, 60-minute integration of time. Joo developed a conversion model based on the effort on collecting rainfall rate data with various integration of time using an Optical Rain Gauge (ORG). Rainwater was not considered instead reserved tank water was used for calibrating the rain gauge whereby the specific gravity was assumed to be 1. The model was developed based only on one location with short duration of rainfall events. Convective rain events were not considered for developing the model. The model is based on power law relationship where the power law curve is the median of the measured data. For higher rainfall rate corresponding to the convective rain events, the model tends to over predict resulting in higher percentage error above 30% for Tropical climates (Joo *et.al.*, 2002).

The maximum rainfall rate used for analysis at 0.01% of time was 80 mm/h. Joo used two ways to express the relationship between the equi-probable rainfall data. The first way is treated as a function of time probability, while the other, as a function of the observed t-minute rainfall rate. Thus the conversion of time probability to 1-minute rainfalls from t-minutes rainfall can be carried out by:

$$P_1 = 1.71 P_t 10^{(-0.242.e^{-t/24.28})} \quad (\text{Joo } et \text{ al, 2002}) \quad (2.13)$$

where

$P_1$  exceeded yearly time probability (%) for 1-minute of time

$P_t$  exceeded yearly time probability (%) for t (5,10,20,60)-minute of time

t integration time in minutes

### 2.6.5 Moupfouma's Method

Moupfouma's method (1995) based on the rainfall rate measurement in Chilbolton (U.K) by the Rutherford Appleton Laboratory (RAL) (ITU-R Doc.5A/39E, 1990-1994) for integration times ranging from 20s to 1 hour using a rain gauge tipping bucket. The measurement is only based in one location with a maximum rainfall rate of 70 mm/h at 0.01% of time that is not appropriate for Tropical climate. Higher rainfall rates above 100mm/h were not consider for calculating the coefficient constant. Moupfouma defined the model as worldwide application only based on the magnitude and shape of the cumulative distribution. The model gave a RMS error above 40% at tropical locations (Migliora *et.al*, 2003; Ong, 1997). Therefore the calculation for rainfall rate  $R(1\text{min})_p$  exceeded during a certain percentage of time for 1 minute integration of time is given as

$$R(1\text{ min})_{0.01} = (R(t\text{ min})_{0.01})^{0.987(t(\text{min}))^{0.061}} \quad (\text{Moupfouma, 1995}) \quad (2.14)$$

where

$R(1\text{ min})_{0.01}$  the rainfall rate (mm/h) for 1-minute at 0.01 percentage of time

$(R(t\text{ min})_{0.01})$  the rainfall rate, (mm/h) at certain integration of time at 0.01 percentage of time

## 2.7 One-minute Rainfall Rates Models

One-minute rainfall rate models are presented where these models require input climatic data and identification of the applicable regions.

### 2.7.1 Dutton and Dougherty Rainfall Rate Model

The Dutton and Dougherty (D-D) rain model (1974) is based on rainfall data for 249 stations grouped into ten climatic rainfall zones covering Europe. The model facilitates error analysis of the predicted distribution, and simplifies procedures for